DETERMINATION OF FIBRE STIFFNESS FROM COMPACTION AND TENSILE TESTS OF UNIMPREGNATED WOOD-FIBRE MATS

R.C. Neagu[1,2], E.K. Gamstedt[1,2] and M. Lindström[2]

[1] KTH Solid Mechanics, Royal Institute of Technology, Osquars backe 1, SE-100 44 Stockholm, Sweden

[2] STFI-Packforsk AB, Box 5604, SE-114 86 Stockholm, Sweden

ABSTRACT

Wood fibres offer excellent specific properties at low cost and are of interest as reinforcement in composites. This work compares two alternative test methods to determine the stiffness of wood fibres from simple macroscopic tests on fibre mats. One method is compression of the fibre mat in the thickness direction which uses a statistical micromechanical model based on first order beam theory to describe the deformation. The other method is tensile testing of fibre mats and back calculation of the fibre stiffness with a laminate model. Experiments include compression and tensile stiffness index tests as well as determination of fibre content, orientation and dimensional distribution. For mats with unbleached softwood kraft fibres, a Young's modulus of 20.1 GPa determined by the compression method compares relatively well with values of 17.4-19.0 GPa obtained from tensile tests. These are also in agreement with values for similar cellulosic fibres found in literature. The compression method is appropriate for low-density fibre mats and while the tensile test works better for well-consolidated high-density fibre mat. The two methods have different ranges of applicability and are complementary to one another. Limitations of the methods are also discussed. The main advantage of the methods is that they are quantitative. The potential as stiffening reinforcement of various types of fibres can then be systematically investigated, even if the fibre mat microstructures are different.

1. INTRODUCTION

Wood and cellulose-fibre composites are finding increased use in load-carrying applications since they offer excellent specific properties at potential low cost. Wood fibres come from a renewable raw material with almost unlimited availability. They are generally lighter, recyclable, biodegradable and have lower ash content after incineration. Drawbacks with cellulose-based fibres are their sensitivity to moisture and large variability in properties. The moisture sensitivity derives from the abundance of hydroxyl groups in the cellulosic material [1]. The large variability is explained by differences in fibre structure due to the overall environmental conditions during growth [2].

The main engineering properties of composites to consider at the material selection stage are stiffness, hygroscopic dimensional stability, strength and fracture toughness. For structural applications with cellulose based composite materials, the most relevant properties are probably stiffness and dimensional stability. To effectively predict the elastic properties of a composite for a specific application it is essential to know the elastic properties of the reinforcing fibres. Investigation of the hygroexpansional properties of wood fibres has been presented in a previous paper [3]. In this accompanying paper the stiffness property of wood fibres for composites is focussed on.

At an early stage in the product development chain it is enviable to determine what kind or which type of wood fibres that have the best potential as reinforcement. The straightforward way to characterize the elastic properties of the fibres is by direct testing of individual fibres. However single fibre tests are very time-consuming and show daunting variability meaning that an enormous amount of tests have to be done to acquire reliable statistics. This is anticipated since the fibre properties vary with e.g. wood species, position in the tree, fibre separation method, etc. [2, 4] A more efficient way to determine the elastic properties of the wood fibres would be from simple and convenient macroscopic test methods in combination with an appropriate mechanical model. A common approach is to measure macroscopic composite properties and then use a micromechanical model to back-calculate the fibre properties [5, 6]. Since wood fibres are supplied in the form of sheets, fibre mats or preforms, it would be desirable to test these semi-manufactured components before the composite is produced.

Candidate fibre materials could then be screened at an earlier stage in the processing chain and the most suitable type of fibre for a certain application could be singled out. Improved cost effectiveness and a more rational quality control can be achieved. The aim of this work is to compare alternative test-methods to determine the stiffness of wood fibres from simple macroscopic tests on fibre mats. Two candidate methods are illustrated in the following.

2. MICROMECHANICAL STIFFNESS MODELS

Two methods of data reduction are considered for the wood fibre mats, namely (*i*) modelling of the elastic compression of a fibre assembly and (*ii*) use of laminate theory to describe the in-plane elastic behaviour of a fibre mat. These are micromechanical models since they use the fibre properties on the microscale to link the microscopic deformation mechanisms to the macroscopic elastic behaviour of the fibre mat.

2.1. Compression of fibre mats in the thickness direction

The model draws on the seminal work by Toll and Månson [7] and Alkhagen [8]. The applicability of this method is subsequently tested on wood fibre assemblies, where the fibre cross-section shows considerable variability.

The distance between fibre contact points will be large in a fibre mat with relatively low density where the fibres are assumed to be long and be distributed in one plane with an arbitrary orientation. These are prerequisites for the model proposed by Toll and Månson [7], which is based on bending of fibre segments between fibre contact points. The basic idea is that in an assembly of elastic fibres under static compression, the load will be transferred across surfaces of contact between neighbouring fibres. If the contact surfaces are small compared to area of the fibre segment span to the adjacent fibre contact, the surface traction can be represented as pointwise acting forces. The fibre mat can then be represented by a finite number of contact points interconnected by elastically deformating beams.

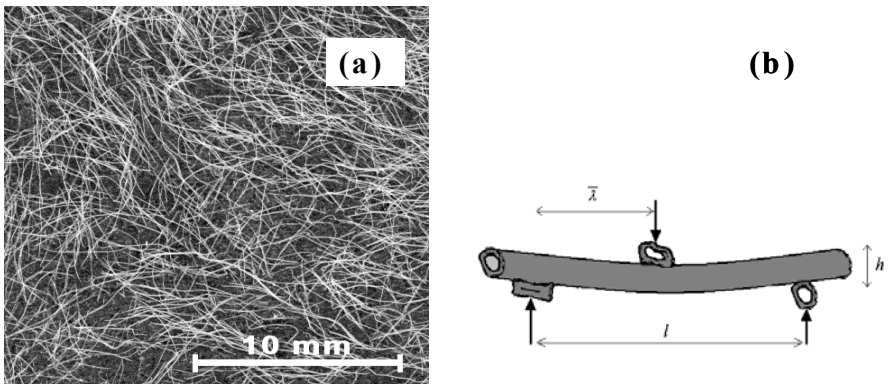

"**Fig. 1.** (a) Structure of a wood fibre mat. (b) Deforming unit, shown with its characteristic measures: height *h* and length *l* which is twice the average contact spacing $\bar{\lambda}$."

In the fibre mat each fibre makes contact with a number of other fibres crossing above and below, see Fig. 1a. When an external uniaxial pressure is applied the fibres act as beams supported at the contact points. The segment of the fibre that deflects between two supporting fibres under the load of a third is termed a deforming unit, Fig. 1b, and can be regarded as a stochastic unit cell [7, 9]. When the network is compressed more fibre contact points are created and the beam segments that provide resistance to compression become shorter and stiffer. The deforming unit defines also the geometry of the fibre network in a way that resembles the microstructure of the fibre mat. Based on statistical probability methods essential model pa-

rameters such as the number of fibre contacts and the distribution of contact spacing in the fibre mat can be estimated [8, 10].

For uniaxial compression Toll and Månson [7] derived the relationship in Eq. (1) between the applied pressure P and the volume fraction of fibres V_f in the network.

$$P = \int_0^{V_\mathrm{f}} \frac{N\langle h\rangle_\mathrm{u}^2}{V_\mathrm{f}\langle s\rangle_\mathrm{u}} \mathrm{d}V_\mathrm{f} \tag{1}$$

where N is the number of deforming units per unit volume, $\langle h\rangle_\mathrm{u}$ is the mean height and $\langle s\rangle_\mathrm{u}$ is the average of the deforming unit compliances ($\langle\cdot\rangle_\mathrm{u}$ denotes average over the number of deforming units). Only elastic reversible deformation is considered. Dissipative mechanisms such as frictional sliding at the contact points and fibre breakage are not taken into account.

By geometrical considerations, it can be shown that the relation $\mathrm{d}V_\mathrm{f}/V_\mathrm{f} = -\mathrm{d}h/h$ implies that the height of the deformation unit h is set equal to the fibre height, denoted H, for low volume fractions [7]. The compliance of a deforming unit can be calculated by using first-order beam theory. If the fibre segment constituting a deformation unit is regarded as a beam loaded at its midsection and fixed at it ends the average compliance can be expressed as

$$\langle s\rangle_\mathrm{u} = \left\langle \frac{1}{192}\frac{l^3}{E_\mathrm{L}I}\right\rangle_\mathrm{u} = \left\langle \frac{1}{24}\frac{\overline{\lambda}^3}{E_\mathrm{L}I}\right\rangle_\mathrm{u} \tag{2}$$

where l, the length of the deforming unit, is substituted with twice the expected contact spacing $\overline{\lambda}$, E_L is the longitudinal elasticity modulus of the fibres and I is the area moment of inertia of the fibre cross-section.

To take the appropriate averages of the parameters in Eqs. (1)-(2) it must be established how the density and distribution of the contact points are related to the fibre volume fraction and the fibre orientation distribution. The theory of Toll [9, 10] and Alkhagen [8] is based on probability arguments that can be readily extended to this work. It is assumed that the fibre orientation distribution $p(\theta)$ and the fibre height distribution $p(H)$ are mutually independent. It is also assumed that fibres are sufficiently long so that the number of deforming units can be considered equal to the number of contact points. Following the derivation of Alkhagen [8] the average of any given quantity taken over all contacts is obtained as

$$\langle\cdot\rangle_\mathrm{c} = \frac{V_\mathrm{f}}{N\langle A_\mathrm{f}\rangle}\langle(\cdot)n_\mathrm{l}\rangle \tag{3}$$

where A_f is the fibre cross-sectional area and n_l is the expected number of contacts per unit length of the a fibre with orientation θ and height H, given by

$$n_\mathrm{l} = V_\mathrm{f}\langle A_\mathrm{f}\rangle^{-1}\left\langle (H+H')\left|\sin(\theta-\theta')\right|\right\rangle = V_\mathrm{f}\langle A_\mathrm{f}\rangle^{-1}\left(H+\langle H\rangle\right)\left\langle\left|\sin(\theta-\theta')\right|\right\rangle \tag{4}$$

Eq. (4) is obtained by introducing a so-called test fibre with an orientation θ and height H. Then if an arbitrary "phantom" fibre with orientation θ' and height H' is considered, a unit length of it will intersect a given unit length of the test fibre only if its centreline lies within a volume of size $(H+H')\left|\sin(\theta-\theta')\right|$. Setting up the number of intersections of the phantom fibres with the test fibre within a certain orientation-height interval $\mathrm{d}\theta'\,\mathrm{d}H'$ and integration over all possible fibre orientations and heights gives the expected number of contacts per unit

length of the test fibre n_l given in Eq. (4). Its reciprocal is the expected contact spacing per unit fibre length, $\bar{\lambda} = n_l^{-1}$. The total number of contacts per unit volume is given in Eq. (5).

$$N = 2V_f^{\,2}\langle A_f\rangle^{-2}\left\langle\left\langle\left|\sin(\theta-\theta')\right|\right\rangle\right\rangle \tag{5}$$

The definition of the double average is found in Ref. [8]. Substituting Eqs. (4)-(5) into Eq. (3) the average among contacts can be rewritten like

$$\langle\cdot\rangle_c = \frac{\left\langle\left\langle(\cdot)(H+H')\right|\sin(\theta-\theta')\left|\right\rangle\right\rangle}{2\langle H\rangle f} \tag{6}$$

where f is an invariant of the fibre distribution orientation [10]. The fibre orientation distribution function $p(\theta)$ can be represented as a normalised Fourier series expansion of the probability density function that reads

$$p(\theta) = \frac{1}{\pi}\sum_{n=0}^{\infty} a_n \cos(2n\theta) \tag{7}$$

with $a_0 = 1$ and the rest of an arbitrary number of Fourier cosine coefficients a_n determined experimentally. The angle θ is the direction for a fibre relative to a predetermined direction, typically the machine direction (MD). Using Eq. (7) with the definition of f in Ref. [7] a closed form expression can be obtained as

$$f = \frac{2}{\pi} - \sum_{n=0}^{\infty}\frac{a_n^{\,2}}{4n^2-1} \tag{8}$$

Assuming that the contact points along a given fibre are randomly spaced the third moment of the expected contact spacing in Eq. (2) can be evaluated as $\overline{\lambda^3} = 6\bar{\lambda}^3$ and then the contact spacing in Eq. (2) can be substituted with its reciprocal. Finally Eq. (6) is applied to Eqs. (1)-(2) which after integration with Eq. (5) results in

$$P = \frac{2\langle A_f\rangle^{-5}\left(\left\langle H^2\right\rangle + \langle H\rangle^2\right)^2 f^4}{5\left\langle I^{-1}\left(H+\langle H\rangle\right)^{-2}\right\rangle} E_f V_f^{\,5} \tag{9}$$

The effects of fibre orientation distribution, fibre segment and variability in fibre dimensions enter the above relationship, Eq. (9), as a direct proportionality factor to the fibre stiffness times the volume fraction of fibres raised to the power of five.

The dimensions of the fibres and their variation are important model parameters and must be determined. Image analysis softwares can be used to determine geometrical parameters such as the cross-sectional areas, perimeter, etc. from micrographs of a fibre mat cross-section (Fig. 2a) Quantities like the area moment of inertia are usually not included in these softwares. It is therefore necessary to estimate the area moment of inertia from measured quantities: fibre area A_f, maximal fibre height H, maximal fibre width W, lumen area A_{lu}, maximal lumen height H_{lu} and maximal lumen width W_{lu}, Fig. 2b. Treating the cross-section as boxed shape would in most cases overestimate the area moment of inertia. It would therefore be better to use the measured quantities and fit a superellipse with the general formula $(y/a)^r+(z/b)^r = 1$ to represent the fibre cross-section. The parameters a and b are given by half

the fibre/lumen width and height, respectively (see Fig. 2b). The parameter r is obtained by fitting to the measured fibre/lumen areas using $A = abrB(r/2,r/2)$, where B denotes the beta function. The area moment of inertia can then be calculated with $I = ab^3B(3r/2,r/2)/2$ [11].

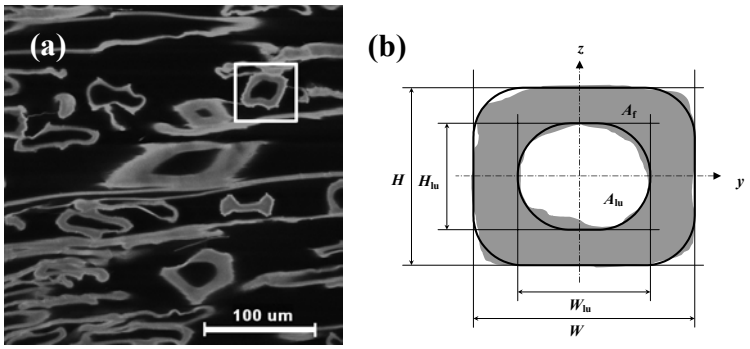

"**Fig. 2.** (a) Confocal microscopy picture of fibre cross-sections. (b) Fibre geometrical parameters used to fit a superellipse to the fibre cross-section."

2.2. Tensile stiffness index of fibre mats

The model outlined above is applicable on fibre mats with low density and long fibres. For fibre mats of fairly high density with strong bonds and long fibres laminate theory can be used to model their in-plane elastic behaviour. The fibre mat can be considered as a homogeneous lamina where an orthotropic constitutive relation describes its in-plane properties. The principal directions of the laminate coincide with the direction of manufacture (MD) and the perpendicular cross direction (CD). The fibres are assumed to be transversely isotropic and uniform, which overlooks the extension-twist interaction and the presence of lumen. The elastic behaviour of an individual fibre embedded in the fibre mat is based on the assumptions outlined by Schulgasser and Page [12] and the components of the fibre stiffness matrix are related to engineering constants as $Q_{11} = E_L/(1 - \nu_{LT}\nu_{TL})$, $Q_{22} = E_T/(1 - \nu_{LT}\nu_{TL})$, $Q_{12} = \nu_{LT}E_T/(1 - \nu_{LT}\nu_{TL})$ and $Q_{66} = G_{LT}$. To account for the inherent porosity of the fibres and the fibre mat the stiffness matrix of the fibre should be multiplied with the volume fraction of the fibres in the fibre mat.

The effective stiffness matrix of a fibre mat with a non-uniform fibre orientation distribution $p(\theta)$ given by Eq. (7) can be obtained through a laminate analogy. Using invariant properties and lamination parameters, a closed-form formulation can be developed for the Young's moduli of the orthotropic fibre mat, E_{MD} and E_{CD}, as a function of the unknown engineering elastic constants of the fibres, viz. E_L, E_T, ν_{LT} and G_{LT}. To reduce the number of unknowns, one can impose certain reasonable relations between these values by comparing different reported data in the literature. Let $R_A = E_L/E_T$ and $R_S = G_{LT}/E_L$ denote the anisotropy ratio and the ratio of shear to the longitudinal elastic modulus, respectively. If the major Poisson ratio is known then E_L can be determined by minimizing the least square sum of the experimentally measured values which gives the following expression

$$E_L = \frac{\rho_f\left(R_A - \nu_{LT}^2\right)\left(E_{MD}^{exp}\dfrac{\partial E_{MD}}{\partial E_L} + E_{CD}^{exp}\dfrac{\partial E_{CD}}{\partial E_L}\right)}{\rho\left(f_{11}f_{22} - f_{12}^2\right)\left(f_{22}^{-1}\dfrac{\partial E_{MD}}{\partial E_L} + f_{11}^{-1}\dfrac{\partial E_{CD}}{\partial E_L}\right)} \tag{10}$$

where ρ is the density of the fibre mat and ρ_f the density of the fibres and f_{11}, f_{22} and f_{12} are functions that include the effect of anisotropy and fibre orientation and can be written

$$f_{11} = \frac{1}{4} a_1 (R_A - 1) + \left(1 - \frac{a_2}{2}\right)\left[\frac{\nu_{LT}}{4} + \frac{R_S}{2}\left(R_A - \nu_{LT}^2\right)\right] + \frac{1 + R_A}{8}\left(3 + \frac{a_2}{2}\right)$$

$$f_{22} = \frac{1}{4} a_1 (1 - R_A) + \left(1 - \frac{a_2}{2}\right)\left[\frac{\nu_{LT}}{4} + \frac{R_S}{2}\left(R_A - \nu_{LT}^2\right)\right] + \frac{1 + R_A}{8}\left(3 + \frac{a_2}{2}\right) \tag{11}$$

$$f_{12} = \frac{\nu_{LT}}{4}\left(3 + \frac{a_2}{2}\right) + \left(1 - \frac{a_2}{2}\right)\left[\frac{1 + R_A}{8} - \frac{R_S}{2}\left(R_A - \nu_{LT}^2\right)\right]$$

where a_1 and a_2 are Fourier cosine coefficients of the distribution function given in Eq. (7). Expressions for the Young's moduli of the fibre mat E_{MD} and E_{CD}, obtained from the inverse of the fibre mat stiffness matrix, are differentiated with respect to E_L. The derivate of E_{MD} can be evaluated as

$$\frac{\partial E_{MD}}{\partial E_L} = \frac{\rho}{\rho_f \left(R_A - \nu_{LT}^2\right)}\left[\left(1 - \frac{R_A}{R_A - \nu_{LT}^2}\right)\left(f_{11} - \frac{f_{12}^2}{f_{22}}\right) + E_L\left(\frac{\partial f_{11}}{\partial E_L} - \frac{f_{12}}{f_{22}}\left(2\frac{\partial f_{12}}{\partial E_L} - \frac{f_{12}}{f_{22}}\frac{\partial f_{22}}{\partial E_L}\right)\right)\right] \tag{12}$$

The expression for the partial derivate $\partial E_{CD}/\partial E_L$ is identical with Eq. (12) but with f_{11} and f_{22} interchanged. The expressions for the partial derivates of the f parameters can be obtained by derivation of the expressions given in Eq. (11). The longitudinal fibre elastic modulus in Eq. (10) can now be determined if the fibre anisotropy ratio, shear to longitudinal elastic modulus ratio, fibre major Poisson ratio and the measured fibre mat elastic moduli are known.

3. EXPERIMENTAL PROCEDURES

Unbleached softwood kraft fibres were used. Hand chipped and screened Norway spruce was cooked and processed according conventional procedures to a kappa number of 46. Fibre mats with a random in-plane fibre orientation distribution were prepared in form of handsheets manufactured according to standard ISO 5269-1:1998. Oriented fibre mats were prepared from the pulp sample using a dynamic sheet former. Detailed process parameters are given in Ref. [3]. Different orientation distributions were used to illustrate the generality of the methods with respect to fibre orientation. Four quadratic specimens with a side length of 50 mm were cut out from the isotopic fibre mat for compressive testing. One specimen was subsequently used to confirm that the orientation distribution of the handsheet was uniform. From the oriented fibre mats specimens were made for tensile testing with dimensions of 100 mm × 15 mm cut both along the MD and the CD.

The grammage was determined according to standard ISO 536:1995. To define the density the structural thickness of the fibre mats was measured. The fibre content in the fibre mats can be determined as the ratio ρ/ρ_f. The fibre orientation distribution was determined by a tape-splitting technique [3]. Two individual layers, the topside and the wire side, were analysed. Image analysis software was employed to determine the orientation distribution. To determine the cross-sectional geometry of the fibres confocal laser scanning microscopy was used. Cross-sectional parameters were obtained in form of the maximum and minimum fibre height and width, maximum and minimum lumen height and width, fibre cell wall area and thickness, lumen area, fibre and lumen perimeter.

An MTS testing machine with a load cell of 40 kN in load control was used for compressive testing. Two parallel plates were pressed together with the fibre-mat specimen in between them while the load and displacement were recorded. The specimens were compressed to a load of 1 kN in 0.5 s. The distance between the press platens was measured as the mean value of the signals from two eddy current transducers (Kaman Multi-Vit) at a sampling rate of 100 Hz. The fibre volume fraction V_f could be determined directly from the distance

between the press platens since the grammage and cell-wall density were known. The tensile stiffness index, defined as the Young's modulus divided by the fibre mat density ρ,was measured according to standard SCAN-P 67:93, using a paper tensile tester by Lorentzen & Wettre AB. All experiments were performed at room temperature and relative humidity of 50%.

4. RESULTS AND DISCUSSION

For the isotropic and oriented fibre mats, the grammage was determined to 185 g/m^2 and 187 g/m^2, respectively. The thickness measurements resulted in an initial thickness of 0.616 mm for the isotropic fibre mat and a thickness of 0.557 mm for the oriented fibre mat. This implies that the isotropic fibre mat had an initial density of 300 kg/m^3 which is slightly lower than the density of the oriented fibre mat of 336 kg/m^3.

Fibre orientation measurements on the isotropic fibre mat were made to confirm that the fibre orientation distribution was uniform. Results obtained for the wire side and top side of the fibre mat shown in Fig. 3a demonstrate a near-uniform distribution. The Fourier cosine coefficients of the distribution function of the fibre orientation distribution a_1 and a_2 can assumed to be zero.

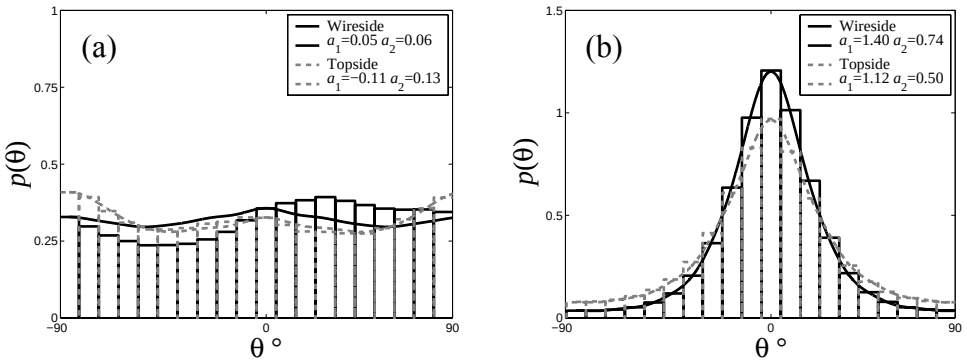

"**Fig. 3.** Fibre orientation distribution of the wire side and top side of (a) the isotropic fibre mat and (b) the oriented fibre mat."

The through-thickness orientation distribution of the oriented fibre mat has been presented by Neagu et al. [3]. In Fig. 3b the measured orientation distribution histogram with a corresponding fit to the orientation distribution function given by Eq. (7) is shown for the wire and top side of the oriented fibre mat. For the purpose of this work average values for the orientation parameters, $a_1 = 1.26$ and $a_2 = 0.62$, suffice to account for the influence of the fibre orientation.

To obtain the necessary geometrical parameters of the fibre cross-section a total amount of 215 fibres from 40 confocal micrographs were analysed. Only fibres perpendicular to the plane of the specimens made from the isotropic fibre mat were considered.

"**Table 1.** Log-normal distribution parameters of fibre geometrical parameters."

Parameter	H (μm)	W (μm)	A_f (μm^2)	I (10^3·μm^4)
μ	2.44	3.84	5.93	8.46
σ	0.74	0.39	0.50	1.95

A log-normal distribution can be used to represent the distribution of wood fibre dimensions. Results are summarised in Table 1 as estimated log-normal distribution parameters, μ (mean of logarithm value) and σ (corresponding standard deviation), of geometrical parameters: fibre height H, fibre width W (see. Fig. 2b), cross-sectional fibre area A_f and the calculated area moment of inertia I. Kolmogorov-Smirnov goodness-of-fit tests were performed to verify that the cross-section dimensions follow a log-normal distribution at a significance level of 5%. The Kolmogorov-Smirnov statistic also showed that the log-normal distribution is generally a better candidate than the Weibull distribution for the measured dimensions.

4.1. Compaction results

Compaction test results for one of the specimens are shown in Fig. 4a. The density of the fibre wall ρ_f can be assumed to be 1500 kg/m^3 [13]. The density of the fibres was estimated as ρ_f times a correction factor to include the lumen with unchanged volume, since the deformation mechanism is beam bending and no fibre cell compression is allowed. A correction factor of 0.77 was calculated as the average of the ratios of fibre wall area to total fibre area including the lumen.

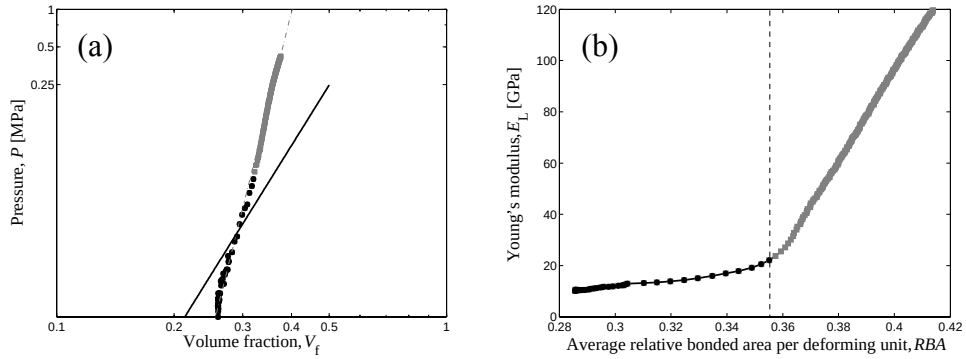

"**Fig. 4.** (a) Pressure vs. volume fraction shown in logarithmic scale. (b) E_L vs RBA."

The longitudinal Young's modulus of the fibres could be obtained by fitting the power law expression given in Eq. (9) to the experimental data in Fig. 4a. Fitting of an arbitrary power law function (dashed-dotted grey line in Fig. 4a) resulted in an exponent higher then the expected exponent of 5. The fix exponent value is a consequence of the chosen deformation mechanism of elastic bending of fibre segments between fibre-fibre contact points. Madsen and Lilholt [14] performed several successive compaction cycles on isotropic hemp, jute and flax fibre assemblies and showed that the exponent almost doubled at the second compaction cycle reaching values larger then 5. It should be noted that the fibre mats used in this study are pressed before dried, as is common practice in manufacture of handsheets. Another contribution to a high exponent is fibre slippage [9]. In case Eq. (9) is fitted to all data points the predicted fibre moduli become unreasonably high. This could be explained by the rather high density of the tested fibre mat, which gave an initial V_f as high as 0.26. An assumption in the model is that the distance between the fibre-fibre contact points is large. When V_f increases the distanced between the fibre-fibre contact points decreases. The key assumption of the model that the surface traction can be represented as pointwise acting forces might not be valid. First order beam theory might not be able to describe the deformation mechanism and other theories that incorporate e.g. shear deformation must be considered. Other deformation mechanisms such as compression of the fibre wall are more likely to step in which could also be an explanation to the stiffer behaviour of the model [15]. It is also probable that local deformation becomes inelastic which ultimately leads to fibre breakage or crushing.

To exclude higher order elastic effects and dissipative mechanisms such as frictional sliding and fibre breakage, the experimental data was truncated. Eq. (4) was used to calculate the average of the expected number of contact points per unit length of a fibre and its inverse gave the average length a deforming unit l (see Fig. 1b) as functions of V_f. The ratio between the mean width of the fibres and the average segment length could be used as an average measure of the 'relative bonded area' per deforming unit, denoted RBA [16]. An approximately linear relationship between V_f and RBA was obtained. In Fig. 4b the effective Young's modulus of the fibres E_L is shown. It can be seen that the fibre stiffness is almost constant up to a critical RBA value (marked by the dashed line at the knee point in Fig. 4b) where the stiffness rises drastically. The critical RBA value and the corresponding V_f value were used to truncate the experimental data. In Fig. 4a the data points marked with black squares are used to fit to Eq. (9), black line of slope 5 in a double-logarithmic plot. The experimental data show a notably steeper slope than expected. This strain hardening effect could be attributed to straightening of curled fibres. The results from the other specimens were treated in the same way and the resulting average of all tests for Young's modulus of the fibres was 20.1 GPa with a standard deviation of 1.9 GPa.

4.2. Tensile test results

The tensile stiffness index was determined to 9.71 (0.60) MNm/kg in the longitudinal direction of the fibre mat and to 1.03 (0.16) MNm/kg in the CD. These are average values and standard deviations (given in parentheses). The volume fraction of the fibres in the fibre mat was 0.22. Before using the laminate micromechanics model, Eqs. (10)-(12), to estimate the stiffness of the fibres from the measured tensile stiffness indices, values of $R_A = E_L / E_T$, and $R_S = G_{LT} / E_L$ must be established. Based on the review of literature data on the anisotropic elastic properties of wood fibres in Ref. [3] a suitable range of stiffness ratios is selected. The ratio, E_L / E_T, ranges from 2 to 10 and G_{LT} / E_L is chosen to 0.1. The major Poisson ratio is set to $\nu_{LT} = 0.3$ [4]. The variation of the longitudinal Young's modulus of the fibres with the anisotropy ratio is not exceedingly large – from 17.4 GPa to 19.0 GPa.

The value of the longitudinal Young's modulus obtained in this study, 17.4-20.1 GPa for unbleached softwood kraft fibres, can be compared with values for similar cellulosic fibres found in literature. For fibres from Norway spruce, Scotch pine and Dogulas fir, various Young's moduli in the dry state ranging from 13 to 25 GPa have been reported [17].

4.3. Comparison of methods

The Young's modulus of the fibres of 20.1 GPa determined with the micromechanical compression model of compares relatively well with the values of 17.4-19.0 GPa obtained by means of back calculation from the macroscopic elastic properties of the fibre mat. Although the methods are fundamentally different with different applicability they provide quantitative results since the fibre volume fraction, orientation distribution and fibre dimensional variability are taken into account. This is the main advantage with using these types of methods as the potential of various types of fibres can be investigated, even if the microstructures are different. The two methods are complementary, since the compression method is appropriate for low-density fibre mats and while the laminate model works better on high-density fibre mat.

There are some matters of concern regarding the applicability of the two methods. The compaction method assumes point loads of Bernoulli-Euler beams. At high volume fractions, shear deformation and transverse fibre compression need to be taken into account. Since the fibres are elastically unbalanced due to their helical microstructure and they are frequently kinked, twisting of fibres is also a likely deformation mechanism which is not modelled at this stage. As for the tensile test of fibre mats, the laminate model assumes a dense packing of fibres and efficient stress transfer along the entire fibre lengths. The two tests are suitable at mutually exclusive microstructures. The aim of the present study was to investigate the applicability of the test methods to determine the fibre stiffness. Since fibre mats of the approxi-

mately the same density were used for the two tests, it is noteworthy to see that the estimated Young's moduli of the fibres were relatively close, despite the difference in model assumptions. It is probable that the investigated fibre mats have a microstructure somewhere between the two extremes, and that the estimated fibre stiffness should fall in the small range between the two estimations.

5. CONCLUSIONS

The effective stiffness of wood fibres has been determined from compaction and tensile tests of unimpregnated wood-fibre mats. A micromechanical approach was used to account for the volume fraction, orientation distribution and dimensional variability of the fibres. In this way quantitative results can be obtained and used to evaluate the potential stiffness contribution of different types of wood fibres for reinforcement in composites. The range of applicability for the compression model is limited to low-density fibre mats of fibres with high aspect ratio. For high-density fibre mats with strong bonds and long fibres an in-plane tensile test and a laminate model are more appropriate. The macroscopic stiffness properties of the fibre mat are then needed input parameters. Results from the two methods compare well despite the difference in assumptions of the two models. Obtained values for the longitudinal Young's modulus ranged from 17.4-20.1 GPa for unbleached softwood kraft fibres are in agreement with values for similar cellulosic fibres found in literature.

References

1. **Uesaka, T.,** "Dimensional stability and environmental effects on paper properties", In: Mark, R. E., ed. *Handbook of Physical and Mechanical Testing of Paper and Paperboard*. New York: Marcel Dekker, (2002), p.115-171.
2. **Haygreen, J. G.** and **Bowyer, J. L.,** "Forest products and wood science". Iowa: The Iowa State University Press, AMES, (1982).
3. **Neagu, R. C., Gamstedt, E. K.** and **Lindström, M.,** "Influence of wood-fibre hygroexpansion on the dimensional instability of fibre mats and composites", Report 361, *KTH Solid Mechanics, Royal Institute of Technology*, Stockholm, Sweden, (2003).
4. **Bergander, A.** and **Salmén, L.,** "The transverse elastic modulus of the native wood fibre wall", *J. Pulp Pap. Sci.*, **26**/6 (2000), 234-238.
5. **Cichocki Jr., F. R.** and **Thomason, J. L.,** "Thermoelastic anisotropy of a natural fiber", *Compos. Sci. Technol.*, **62**/5 (2002), 669-678.
6. **Nordin, L.-O.,** "Wood fiber composites: From processing and structure to mechanical performance", Doctoral Thesis, *Deparment of Applied Physics and Mechanical Engineering*, *Luleå University of Technology*, Luleå, Sweden, (2004).
7. **Toll, S.** and **Månson, J.-A. E.,** "Elastic compression of a fiber network", *J. Appl. Mech.-T. ASME*, **62**/1 (1995), 223-226.
8. **Alkhagen, M. I.,** "Nonlinear elasticity of fiber masses", Doctoral Thesis, *Department of Applied Mechanics*, *Chalmers University of Technology*, Göteborg, Sweden, (2002).
9. **Toll, S.,** "Packing mechanics of fiber reinforcement", *Polym. Eng. Sci.*, **38**/8 (1998), 1337-1350.
10. **Toll, S.,** "Note: On the tube model for fiber suspensions", *J. Rheol.*, **37**/1 (1993), 123-125.
11. **Jaklic, A.** and **Solina, F.,** "Moments of superellipsoids and their application to range image registration", *IEEE T. Syst. Man Cy. B*, **33**/4 (2003), 648-657.
12. **Schulgasser, K.** and **Page, D. H.,** "The influence of transverse fibre properties on the in-plane elastic behaviour of paper", *Compos. Sci. Technol.*, **32**/4 (1988), 279-292.
13. **Kajanto, I., Laamanen, J.** and **Kainulainen, M.,** "Paper bulk and surface", In: Niskanen, K., ed. *Paper Physics*. Helsinki: Fapet Oy, (1998), p.89-115.
14. **Madsen, B.** and **Lilholt, H.,** "Compaction of plant fibre assemblies in relation to composite fabrication", In: *Proceedings of the 23rd Risø International Symposium*. Lilholt, H., et al. ed. Risø, Denmark, (2002), p. 239-250.
15. **Provatas, N.** and **Uesaka, T.,** "Modelling paper structure and paper-press interactions", *J. Pulp Pap. Sci.*, **29**/10 (2003), 332-340.
16. **Sampson, W. W.,** "The statistical geometry of fractional contact area in random fibre networks", *J. Pulp Pap. Sci.*, **29**/12 (2003), 412-416.
17. **Ehrnrooth, E. M. L.** and **Kolseth, P.,** "The tensile testing of single wood pulp fibers in air and in water", *Wood Fiber Sci.*, **16**/4 (1984), 549-566.